2019 International Conference on Robotics and Automation (ICRA)
Palais des congres de Montreal, Montreal, Canada, May 20-24, 2019

Distributed Radiation Field Estimation and Informative Path Planning for Nuclear Environment Characterization

Frank Mascarich, Christos Papachristos, Taylor Wilson, and Kostas Alexis

***Abstract*— This paper details the system and methods designed to enable the autonomous estimation of distributed nuclear radiation fields within complex and possibly GPS–denied environments. A sensing apparatus consisting of three radially placed Thallium–doped Cesium Iodide (CsI(Tl)) scintillators and Silicon Photomultipliers (SiPm) combined with custom–built pulse counting circuitry is designed and the provided readings are pose–annotated using LiDAR-based localization. Given this capacity, a method that utilizes the radiation intensity readings to first calculate the immediate field gradient and then combine this information to update and co-estimate the believed field intensity and gradient across the whole environment is developed. The strategy propagates the effect of each local measurement through field gradient co-estimation and simultaneously derives a model of the underlying uncertainty. To further support the need for informative data gathering, especially in the framework of emergency and rapid reconnaissance missions, a path planning strategy is also developed that first utilizes the field intensity and uncertainty estimates to select its new waypoint and then performs terrain traversability analysis to derive admissible paths. The complete system is evaluated both in simulation and experimentally. The experimental results refer to the autonomous exploration and field estimation inside an indoor facility within which actual radioactive uranium and thorium ore sources have been distributed.**

I. INTRODUCTION

Nuclear energy continues to play a major role in our societies. About 11% of the world's electricity is produced from approximately 450 active nuclear reactors. In about 225 research reactors, 50 countries utilize nuclear energy not only for research but also for the production of medical and industrial isotopes, as well as for training [1]. Over $27,000$ nuclear weapons exist in the world and thousands are deployed on land, at sea and in the air. The U.S. Nuclear Weapons Complex alone refers to a multitude of specialized facilities responsible for storage, processing, maintenance and other activities in support of the nuclear arsenal. Use of nuclear sources is a *de facto* reality of our times. Radiological measurement and surveying, source localization and field mapping are therefore tasks of paramount importance and unparalleled value in scenarios ranging from environmental contamination, monitoring the sites of nuclear waste storage, as well as illicit and lost source retrieval. In response to these facts, in this work we examine the problem of autonomous mapping of distributed nuclear radiation fields which corresponds to a major challenge in a variety of critical missions related to surveillance, environment characterization, illicit source identification and other security tasks.

This material is based upon work supported by the Department of Energy under Award Number [DE-EM0004478].

The authors are with the Autonomous Robots Lab, University of Nevada, Reno, 1664 N. Virginia, 89557, Reno, NV, USA fmascarich@nevada.unr.edu

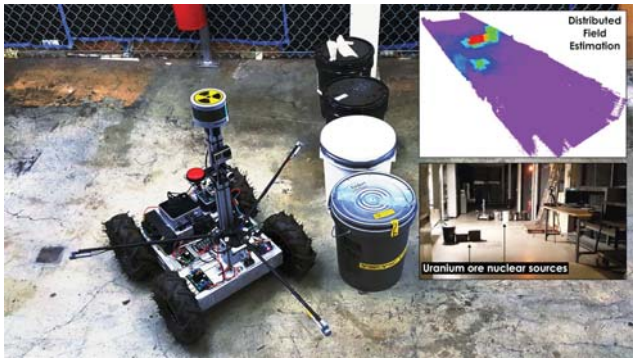

Fig. 1. Instance of a GPS–denied distributed nuclear radiation field estimation mission. The proposed solution enables the robust estimation of complex radiation fields and the autonomous mission execution through informative path planning.

In the literature, multiple efforts relate to the problem of automatically guided or teleoperated robots [2–4] operating in open–ended and GPS–supported environments [2, 5] conducting single radiation source localization. However, the problem of autonomous distributed nuclear radiation field mapping is not studied to an equal extent. Furthermore, the robotic systems utilized in the framework of radiological surveying are not characterized by advanced autonomy and typically fail to operate and intelligently gather information in complex, cluttered, often highly contaminated and GPS–denied nuclear sites. However it is these exact conditions in terms of radiation field distribution and environment complexity that are of true interest and importance. Iconic examples include the "sarcophagus" of Chernobyl's Unit 4 and its surroundings, the Fukuhshima Daiichi nuclear power plant, and the need to inspect waste disposal areas or environments subject to irregular radiation levels.

Motivated by the above, this work contributes the full algorithmic design and system implementation of a solution for autonomous robotic distributed nuclear radiation field mapping in possibly GPS–denied environments. At first, a probabilistic approach to the problem of estimating a distributed radiation field is developed exploiting three radially–placed detectors on–board the robot. To ensure efficient autonomous field estimation, we further propose an active path planning strategy that identifies the most informative waypoints to gather additional radiological data and ensures reliable and robust field estimation. Provided this capacity, an autonomous ground rover, called "RadMapper",

978-1-5386-6027-0/19/$31.00 ©2019 IEEE

is developed and integrates three miniature Thallium-doped Cesium Iodide (CsI(Tl)) scintillators combined with Silicon Photomultipliers (SiPM), in–house developed pulse counting circuitry, LiDAR–based localization and mapping, terrain traversability analysis towards admissible path planning and reliable guidance, alongside the required control systems and low–level electronics. The proposed solution is tested experimentally in complex environments integrating *real* nuclear radiation sources, specifically a mixture of raw, unprocessed uranium and thorium ore.

The remainder of the paper is structured as follows: Section II overviews related work, while the problem of autonomous distributed radiation field estimation is defined in Section III. The proposed solution is detailed in Section IV, followed by a description of the "RadMapper" in Section V. Experimental results are presented in Section VI, while conclusions are drawn Section VII.

II. RELATED WORK

The area of radiation field mapping and source localization has been studied through a set of contributions such as [6–10]. Among them, maximum likelihood estimation is utilized in [8, 10], numerical adjoints in conjuction to a bayesian formulation are used in [6], while a particle filter is employed in [7]. These strategies are primarily focusing on the problem of estimating a single or at least multiple discrete sources and tend to assume that a large number of radiation measurements are available - typically provided by a fixed array of sensors. For the case of distributed field estimation, existing work has primarily focused on non–nuclear applications relying on the deployment of wireless sensor networks [11, 12], while relevant robotics research exists but is less common [13]. Active source (e.g. radiological, chemical) localization has been studied in [14–16]. In the specific field of nuclearized robotics, a set of works [2, 3, 5, 17–20] have presented interesting results. The authors in [17] describe a distributed guidance strategy by means of information gradients to estimate the distribution of radiation and test their method using light as a "radiation analog" source. The works in [18, 20] aim to handle multiple sources and evaluate their methods in simulation. The authors in [2] employ semantic scene segmentation based on aerial robotic data in order to better inform the information gathering trajectories of a ground robot (and broadly an aerial-ground robot team). The work in [19] uses a helicopter UAV to map radiation over large environments. The contribution in [5] refers to post–disaster radiation mapping also using a helicopter UAV combined with a grid–based bayesian estimator for single source localization and contour analysis for multiple source handling. Our previous work in [21] emphasizes single–source localization assuming only a sparse set of measurements automatically collected from a Micro Aerial Vehicle. In relation to these efforts, this paper contributes a) the design of an estimation algorithm tailored specifically to the complex case of distributed nuclear radiation fields, b) the design of an active path planning strategy which ensures that the next–most–informative waypoint is identified and the robot therefore efficiently maps radiation fields in areas that are initially completely unknown, as well as c) the development, experimental realization, and validation of a robotic system that integrates a three–detector apparatus and the necessary GPS–denied localization, terrain traversability analysis and control laws that enable the autonomous exploration, radiation field estimation and area mapping within environments for which no prior knowledge is available. The developed solution is tested in real-life field experiments involving actual nuclear radiation sources.

III. PROBLEM DESCRIPTION

The first problem considered in this work is that of estimating the underlying spatial distribution of a nuclear radiation field within an initially unknown map of the environment. Considering an iterative solution to this problem and the co–estimation of the field uncertainty, the second problem considered in this work is that of optimized information gathering and specifically the design of a path planner that identifies the next–most–informative waypoint over which radiation data should be sampled in order to best support the aforementioned field estimation process. As a side and highly relevant product of the envisioned operation, a 3D map of the environment, annotated with the estimated radiation field, is also desired. The aforementioned problems are more formally defined below.

Problem 1 (Distributed Radiation Field Mapping) Given a bounded but initially unknown area $\mathcal{S}$ and a set of measurements $\{\boldsymbol{\mu}_m\}$, each of them containing the position $\mathbf{p}_m$ over which the measurement took place and a triplet of radiation measurements $\lambda_m^i, i = 1, 2, 3$ from a corresponding number of radially placed detectors, the goal is to estimate the underlying spatial distribution $\mathbf{M}(\mathbf{p}_t)$ which best fits all data in $\{\boldsymbol{\mu}_m\}$ and accurately predicts the true field distribution at every possible test location $\mathbf{p}_t$ within $\mathcal{S}$.

Problem 2 (Informative Path Planning for Radiation Field Estimation) Given the initially unknown but bounded area $\mathcal{S}$, its iterative exploration and reconstruction of a map $\mathcal{M}$ and the incrementally derived measurements $\{\boldsymbol{\mu}_m\}$ - each of them containing the position $\mathbf{p}_m$ over which the measurement took place and a triplet of radiation measurements $\lambda_m^i, i = 1, 2, 3$ from a corresponding number of radially placed detectors - identify a collision–free path κ_{opt} that incrementally leads to measurements $\boldsymbol{\mu}_m$ such that they are optimized for accurate estimation of the underlying distribution $\mathbf{M}(\mathbf{p}_t)$ of the radiation field at every test location $\mathbf{p}_t$. Feasible paths κ of this problem are subject to the kinematic constraints of the vehicle and traversability limitations of the robot against the terrain.

Beyond the solution to these two problems, an important and necessary component of the operation is a 3D map of the environment and terrain $\mathcal{M}$ in which the mission takes place.

IV. ACTIVE DISTRIBUTED RADIATION MAPPING

This section details the distributed nuclear radiation field estimation method combined with a specialized informative

path planning framework to support the underlying estimation process. As a first step, the employed radiation sensing solution is outlined.

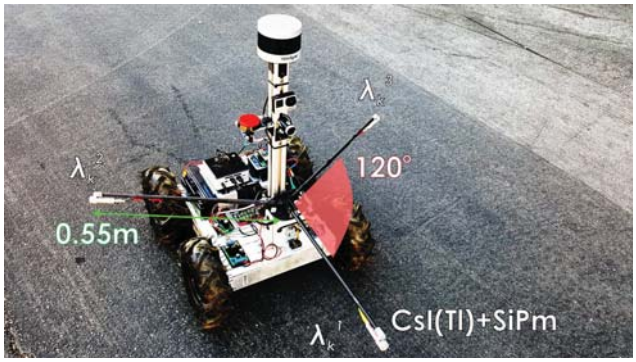

Fig. 2. Illustration of the developed three Thallium-doped Cesium Iodide (CsI(Tl)) scintillators with Silicon Photomultipliers (SiPm) radially placed on–board the RadMapper robot.

A. Radiation Sensing Apparatus

In this work we propose and employ a radiation sensing solution that relies on three miniature Scionix V10B10 Thallium-doped Cesium Iodide (CsI(Tl)) scintillators combined with Silicon Photomultipliers (SiPm) radially distributed on a plane at a 120° angle step size. The mounting point of each detector is 0.55m from the robot body. The motivation behind using co–planar detectors is to enable the immediate calculation of the 2D field gradient. This sensor apparatus is ferried onboard the robot as depicted in Figure 2. The three detectors are interfaced using custom–designed pulse counting and spectroscopy circuitry which weighs 23g. When the robot is at a configuration $\xi_k = [\mathbf{p}_k|\psi_k]$ corresponding to a position $\mathbf{p}_k$ and heading ψ_k, each detector $i \rightarrow 1,2,3$ is at a position $\mathbf{p}_k^i$ and provides a radiation counts reading y_k^i both due to the effect of the background radiation and a set of an arbitrary amount of acting sources $s^j \in \mathcal{S}$ that in their combination correspond to the effect of distributed radiation:

$$y_k^i = T_D^k A e(\sum_j \frac{v_{s^j}}{4\pi||\mathbf{p}_k^i - \mathbf{p}_{s^j}||^2} + v_b),\ i \rightarrow \{1,2,3\} \quad (1)$$

where A and e are the area and the efficiency of the detector, v_{s^j} are the intensity of the sources, $||\mathbf{p}_k^i - \mathbf{p}_{s^j}||^2$ denotes the euclidean distance from the detector to each source s^j, T_D^k is the dwell time over which a measurement is acquired, and v_b is the background intensity. The quantities A and e of Eq (1) are determined by the calibration of the detector in a pre–characterized chamber and for our system the calibration procedure is detailed in our previous work [21]. The background intensity rate v_b can be derived through preliminary measurements away from the expected radiation sources (exploiting the fast decay of the inverse square law). Due to the fact that the measurement process is governed by Poisson distributions, the role of dwelling time is critical to ensure reliable measurements through averaging of the counting statistics. For every dwell position $\mathbf{p}_k^i$, the reading is averaged over T_D^k, background is subtracted and the average value $\lambda_k^i,\ i \rightarrow \{1,2,3\}$ is used for field estimation purposes.

B. Distributed Radiation Field Estimation

The proposed Distributed Radiation Field Estimation algorithm exploits the inverse square property of radiation propagation and the co–planar, radially distributed detectors mounted on the RadMapper system to co–estimate both the intensity of the radiation field at each of the detector positions and the field gradient at their centroid. To accomplish this task, the algorithm maintains a set of grids, each co-located on the area of interest.

At boot time, the algorithm obtains the number of cells in the x-direction n, and the number of cells in the y-direction m, as well as the number of cells per meter θ, as parameters. The grid layers utilized are the measured intensity grid ($\mathbf{M}_R$), the believed intensity grid ($\mathbf{M}_B$), the measured gradient grid ($\mathbf{G}_R$), the believed gradient grid ($\mathbf{G}_B$), the intensity uncertainty grid ($\mathbf{U}$), the gradient uncertainty grid ($\mathbf{\Sigma}$), and the radiation curiosity grid ($\mathbf{C}$). These grids discretize the environment into an array of cells, each of which estimate the respective component of the radiation field in the area contained by the grid cell. $\mathbf{M}_R$, $\mathbf{M}_B$, $\mathbf{U}$, and $\mathbf{\Sigma}$ are defined as $2D$ matrices with dimensions $m \times n$. The gradient grids, $\mathbf{G}_R$ and $\mathbf{G}_B$, are defined as $3D$ matrices with dimensions $m \times n \times 2$, as each cell stores the gradient in the x direction and the gradient in the y direction as distinct quantities.

The algorithm operates in two sequential phases, a measurement phase and a propagation phase. At the start of a mission, the $\mathbf{M}_B$ and $\mathbf{M}_R$ grids are initialized with the background intensity, which is also obtained as a parameter. Similarly, both uncertainty grids, $\mathbf{U}$ and $\mathbf{\Sigma}$ are initialized to 1.0 indicating complete uncertainty. The measurement phase begins when the system obtains new detector readings at 10Hz from the onboard radiation counting system. Using the position estimate from the system's odometry solution, the position of each detector is obtained in the X-Y plane, and the corresponding cell in $\mathbf{M}_R$ is updated with the new readings using a moving average. The algorithm then calculates the instantaneous field gradient from these three new readings using Eq (2), where $\mathbf{p}_k^c - \mathbf{p}_k^i$ denotes the vector from the detector's position to the the centroid of the detector ring $\mathbf{p}_k^c$ on the X-Y plane. This estimated field gradient is added to the $\mathbf{G}_R$ grid cell corresponding to the centroid of the detector ring, again in a moving average manner.

$$\gamma_k = \begin{bmatrix}\gamma^x \\ \gamma^y\end{bmatrix}_k = \frac{1}{3}\sum(\mathbf{p}_k^c - \mathbf{p}_k^i)\lambda_k^i,\ i \rightarrow \{1,2,3\} \quad (2)$$

The propagation phase iterates over all grid cells sequentially. First the $\mathbf{U}$ and $\mathbf{\Sigma}$ grids are updated using Eq (3) and Eq (4), where $N_{i,j}^g$ is the number of gradient measurements obtained at cell i,j and $N_{i,j}^m$ is the number of intensity measurements obtained at cell i,j. Then, for each cell, the $\mathbf{M}_B$ and $\mathbf{G}_B$ grids are updated. At cells for which a sufficient number ($> N_{\min}$) of readings have been obtained, the $\mathbf{M}_B$

grid, and the $\mathbf{G}_B$ grid are assigned the value of the $\mathbf{M}_R$ grid and the $\mathbf{G}_R$ grids respectively. At cells for which the number of readings that have been obtained is less than $N_{\min}$, the algorithm iterates over each of the cell's neighbors and calculates the intensity contribution of each neighbor using their believed intensity and believed gradient by Eq (7), where $\upsilon^N_{m,\ell}$ and $\sigma^N_{m,\ell}$ are the uncertainties of cell m,l re-scaled such that the sum of the intensity uncertainties and the sum of the gradient uncertainties for particular neighborhood both equal 1. The intensity contributions are then averaged and this average is then assigned to the $\mathbf{M}_B$ grid for the cell of interest using Eq (6). Finally, the neighbors' gradients are averaged by Eq (5), and this average is logged in the $\mathbf{G}_B$ grid.

$$\sigma_{i,j} = \frac{|\gamma_{i,j}|}{N^g_{i,j}} \tag{3}$$

$$\upsilon_{i,j} = \frac{\mu_{i,j}}{N^m_{i,j}} \tag{4}$$

$$\gamma_{i,j} = \sum_{m=i-1}^{m=i+1} \sum_{\ell=j-1}^{\ell=j+1} \gamma_{m,\ell}\sigma^N_{m,\ell},\ m \neq i,\ \ell \neq j \tag{5}$$

$$\mu_{i,j} = \sum_{m=i-1}^{m=i+1} \sum_{\ell=j-1}^{\ell=j+1} \mu_{m,\ell\to i,j},\ m \neq i,\ \ell \neq j \tag{6}$$

$$\mu_{m,\ell\to i,j} = \mu_{m,\ell}\upsilon^N_{m,\ell} + \begin{bmatrix} m-i \\ \ell-j \end{bmatrix}^T \gamma_{m,\ell}\sigma^N_{m,\ell}\theta \tag{7}$$

A visualization of the employed field intensity, gradient and uncertainty grids is depicted in Figure 3, while an algorithmic outline of the abovementioned procedure is presented in Algorithm 1.

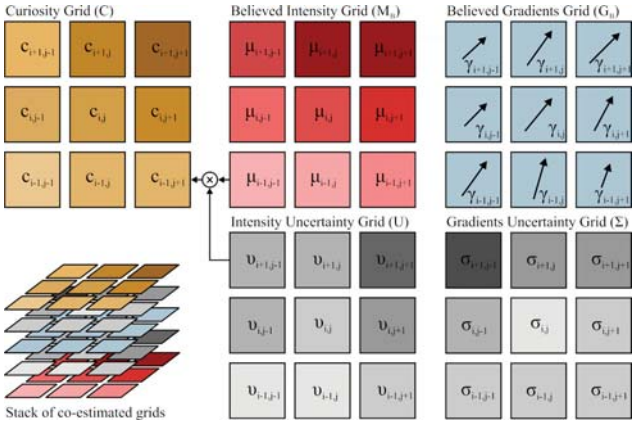

Fig. 3. Visualization of the believed intensity $\mathbf{M}_B$, intensity uncertainty $\mathbf{U}$, believed gradient $\mathbf{G}_B$, gradient uncertainty $\mathbf{\Sigma}$, and curiosity $\mathbf{C}$ grids.

Algorithm 1 Distributed Radiation Field Estimation Iteration given prior $\mathbf{M}_B, \mathbf{U}, \mathbf{G}_B, \mathbf{\Sigma}$ and $\mathbf{M}_R, \mathbf{G}_R$

Acquire new measurements $\{\lambda^i_k\}_{i\to 1,2,3}$
Pose annotate $\{\lambda^i_k\}_{i\to 1,2,3}$ given $\boldsymbol{\xi}_k = [\mathbf{p}_k|\psi_k]$
Augment measurements list $\mathbf{\Lambda}_k \leftarrow \mathbf{\Lambda}_{k-1} \cup \{\lambda^i_k\}_{i\to 1,2,3}$
Augment positions list $\mathbf{P}_k \leftarrow \mathbf{P}_{k-1} \cup \{\mathbf{p}^i_k\}_{i\to 1,2,3}$
Calculate instantaneous field gradient γ_k - Eq (2)
Update measured intensity and measured gradient grids $\mathbf{M_R}, \mathbf{G_R}$
for all grid cells $\mathbf{cell}_{i,j}$ in grids **do**
  Update intensity uncertainty $\upsilon_{i,j}$ at $\mathbf{cell}_{i,j}$ - Eq (3)
  Update gradient uncertainty $\sigma_{i,j}$ at $\mathbf{cell}_{i,j}$ - Eq (4)
  if $\mathbf{cell}_{i,j}$ contains at least $N_{\min}$ measurements **then**
    believed intensity $\mu_{i,j} = \text{mean}(\lambda^i_k \in \mathbf{cell}_{i,j})$
  else
    for all neighbor cells $\mathbf{cell}_{m,\ell}$ of $\mathbf{cell}_{i,j}$ **do**
      Update believed intensity $\mu_{m,\ell\to i,j}$ from $\mathbf{cell}_{m,\ell}$ to $\mathbf{cell}_{i,j}$ - Eq (7)
    end for
    Update believed intensity $\mu_{i,j}$ at $\mathbf{cell}_{i,j}$ - Eq (6)
    Update gradient $\gamma_{i,j}$ at $\mathbf{cell}_{i,j}$ - Eq (5)
  end if
end for
Return Updated grids $\mathbf{M}_B, \mathbf{U}, \mathbf{G}_B, \Sigma$

C. Informative Path Planning for Radiation Field Estimation

The proposed distributed nuclear radiation field estimation algorithm provides at each iteration its best estimate given the collected sensor measurements. However, especially when the estimation task is subject to limited mission time - as it is often the case in emergency response and other rapid reconnaissance applications - it is of particular importance to design a specialized path planning loop that iteratively feeds the estimation process with measurements of optimized informativeness. Such an algorithm is further proposed in the framework of this work. More specifically, the Next-Best-Radiation-Waypoint (NBRW) planner is detailed in Algorithm 2. At each iteration, the algorithm first exploits the calculated believed intensity grid $\mathbf{M}_B$ and intensity uncertainty grid $\mathbf{U}$ to derive a "curiosity" grid $\mathbf{C}$ calculated as the Hadamard product of $\mathbf{M}_B$ and $\mathbf{U}$. The next most informative waypoint ("Radiation waypoint") $\mathbf{p}^{cr}$ is then calculated as the obstacle-free grid location with the highest curiosity value. With the next goal location determined, the algorithm proceeds to build a random tree $\mathbb{T}$ of admissible robot paths by incrementally adding new nodes n over robot configurations ξ_{new}. An admissible path is one that a) is collision-free, b) connects the initial robot configuration ξ_0 consisting of the current robot location $\mathbf{p}_k$ and heading ψ_k with the configuration ξ_{final} that is within a small radius r around $\mathbf{p}^{cr}$ (with any orientation), and c) is traversable as calculated based on a traversability metric $\mathcal{T}(\mathcal{M}, \xi_n, \xi_\ell)$ over the map of the environment and any given robot configurations ξ_n, ξ_ℓ. As this algorithm executes, optimized admissible paths κ_{opt} to the goal location $\mathbf{p}^{cr}$ are incrementally derived

(when at least one exists). As cost metric for the optimization process, the euclidean distance is considered.

Algorithm 2 Next-Best-Radiation-Waypoint - Iteration

$\mathbf{C} \leftarrow \mathbf{M}_B \odot \mathbf{U}$ {Curiosity grid as the Hadamard product of the Intensity and Uncertainty grids}
$\mathbf{p}^{cr} \leftarrow \mathbf{p} : \mathbf{C}(\mathbf{p^{cr}}) == \max(\mathbf{C})$ {Radiation waypoint}
$\xi_0 \leftarrow$ current vehicle configuration
Initialize $\mathbb{T}$ with ξ_0
$c_{\min} \leftarrow c_{init}$ {Initialize with large value c_{init}}
$N_{\mathbb{T}} \leftarrow$ Number of initial nodes in $\mathbb{T}$
while $N_{\mathbb{T}} < N_{\max}$ **or** $c_{\min} == c_{init}$ **do**
  Incrementally build $\mathbb{T}$ by adding new $n_{new}(\xi_{new})$
  $N_{\mathbb{T}} \leftarrow N_{\mathbb{T}} + 1$
  if New admissible paths exist **then**
    Evaluate new best path κ_{opt} with cost c_{opt}
    $c_{\min} \leftarrow c_{opt}$
  end if
end while
Return κ_{opt}

V. RADIATION MAPPING ROVER

This section overviews the RadMapper system design for all its functionality apart from the radiation measurement solution described in the previous section. A diagram of its software architecture is shown in Figure 4.

A. RadMapper Rover

The developed RadMapper is built around a SuperDroid IG52-DB4 4WD roving platform. The integrated low–level electronics drive the system in skid-steer mode, while a NUC5i7RYH provides high–level computation resources and is interfaced with all sensing systems and the low–level electronics responsible for the vehicle actuation. A simple differential–drive controller is implemented and drives the system in a manner such that the heading difference to the goal configuration is corrected with priority at 20Hz.

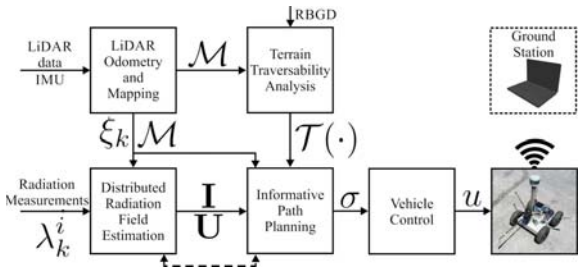

Fig. 4. Overview of the functional modules of the RadMapper rover.

B. Localization and Terrain Mapping Solution

To enable GPS–denied localization and mapping, RadMapper integrates a Velodyne Puck LITE 16–channel LiDAR with vertical and horizontal field of view equal to 30° and 360° respectively and a nominal range of 100m. Utilizing an implementation of the LiDAR Odometry And Mapping (LOAM) method in [22] the robot full pose $\boldsymbol{\zeta}_k$ consisting of its position $\mathbf{p}_k = [x, y, z]$ and its orientation $\boldsymbol{\eta}_k = [\phi, \theta, \psi]$, alongside a point cloud representation $\mathcal{M}$ of the environment are estimated. Given the pose $\boldsymbol{\zeta}_k$ and the registered point cloud map $\mathcal{M}$ at every iteration the robot further fuses the data from an oblique facing Realsense D435 RGBD sensor to derive a higher resolution representation of the terrain therefore enhancing $\mathcal{M}$. Subsequently, terrain traversability analysis between any two candidate robot configurations is enabled using the Elevation Mapping framework in [23–25]. These functionalities are essential for the autonomous navigation of the robot especially in the case of indoor, cluttered environments and rough terrain.

C. Additional Payload

RadMapper integrates additional subsystems relevant to its mission profile. In particular, the robot further integrates two front facing cameras (with fisheye and traditional lenses), and two independent communication channels for short range high–bandwidth data transfer (2.4GHz), long–range telemetry (915MHz) and fall-back remote control.

VI. EVALUATION STUDIES

In order to systematically evaluate the proposed distributed nuclear radiation field estimation and informative path planning methods, alongside the overall operation of the RadMapper robot, a set of studies both in simulation and experimentally were conducted. The simulation studies serve to verify the performance trends of the algorithms, while the experimental analysis allows comprehensive evaluation in real world conditions. In the conducted experiment, true nuclear radiation sources were utilized. An open dataset is released [26] and includes raw radiation readings, pose estimates, ground–truth of the estimated field and the results of our solution for nuclear field estimation.

A. Simulation Studies

Prior to the experimental evaluation of the proposed solution for robotic nuclear radiation field mapping, a simulation study was conducted to evaluate the combined performance of the estimation and planning methods. More specifically, considering an environment involving a complex radiation distribution, we simulated the performance of an ideal robot (ideal unconstrained motion) integrating three radially distributed radiation detectors (at a radius of 0.55m) for which modeling of Poisson noise was accounted. The derived estimation of the underlying distributed radiation field is depicted in Figure 6 alongside comparison with model "ground–truth". This result serves to demonstrate and verify the potential of the proposed methods prior to the experimental deployment and evaluation.

B. Experimental Evaluation

The RadMapper was tested inside a complex workshop–like environment within which distributed nuclear radiation sources were deployed. These radiation sources were assembled using a mixture of raw, unprocessed uranium and

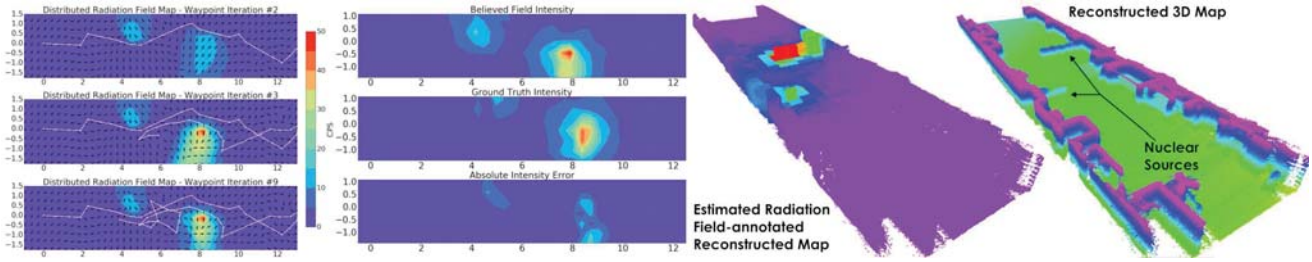

Fig. 5. Final results and steps of the execution of the proposed distributed field estimation and informative path planning methods. On the left, three iterations of the execution of the planner are depicted alongside the estimated nuclear radiation field at every point in time. xy axes correspond to meters, while the color value represents radiation intensity as measured in terms of Counts Per Second (CPS). The tendency of the planner to select points along the complete environment and close to areas of high intensity (or uncertainty) is depicted. As shown on the second column, after the 9th iteration, the methodology manages to estimate a very accurate representation of the radiation field as verified through the ground-truth and error plots. Ground–truth is derived by exhaustively acquiring measurements in the environment following a very dense grid and dwelling for long periods at every point so as to minimize the uncertainty imposed by the Poisson distribution governing radiation. On the right side, the derived reconstruction of the environment is presented, first color–annotated with radiation intensity levels and subsequently based on a height–colormap. We intentionally present the reconstruction only up to a height of 0.6 meters to show the presence of the deployed and distributed radioactive uranium and thorium ore buckets.

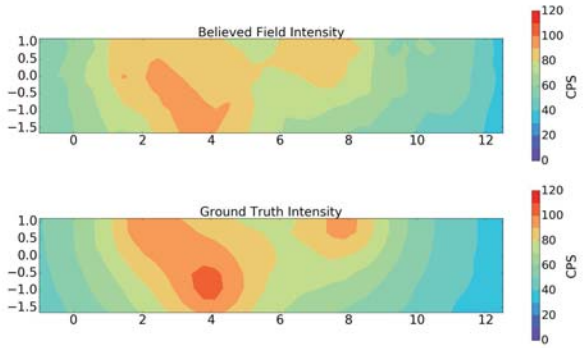

Fig. 6. Simulation based result on the estimation of a complex nuclear radiation field based on 300 radiation waypoints selected by the NBRW planner and executed by an "ideal robot" with no kinematic or dynamic constraints (i.e., measurements gathered exactly at planned location). This result serves to demonstrate the performance of the distributed radiation field estimation method. As shown, the reconstructed field estimates lead to a result very close to that of the modeled radiation field ("ground–truth"). Measurements are shown in Counts Per Second (CPS).

thorium Ore. The RadMapper was commanded to enter this initially unknown environment and conduct a rapid reconnaissance mission in which it a) estimates the underlying radiation field, while simultaneously b) building a 3D map of its surroundings. This experiment evaluates both the robustness of the field estimation method due to the complexity of real sources and the information gathering behavior of the robot enabled by the NBRW planner, as well as the overall functionality of the system with respect to the accuracy of the integrated nuclear radiation measurement solution and its capacity to traverse terrain that imposes mobility constraints. Figure 5 presents a) the estimated radiation field based on the robot mission alongside a manually reconstructed ground–truth map of the field, b) the planned paths commanded by the NBRW informative path planner and executed by the robot, and c) the reconstructed 3D and radiation–annotated model of the environment. As presented, the proposed approach achieves accurate estimation of the distributed radiation field after a small set of robot trajectories to autonomously gather data. This capacity has the potential to prove critical in a variety of inspection, decommissioning, emergency response and security applications.

VII. CONCLUSIONS

This paper presents a comprehensive solution for the problem of autonomous estimation of distributed nuclear radiation fields in possibly GPS–denied environments. It employs a radiation sensing apparatus that consists of three radially placed scintillators therefore having the potential of instantaneous gradient calculation on a plane. A probabilistic method that simultaneously estimates the believed radiation intensity and the field gradient alongside their underlying uncertainties is developed and combined with an informative path planning approach for optimized measurement acquisition and collision–free navigation. The solution is integrated on–board the RadMapper robot, a system that relies on LiDAR-based localization and terrain traversability analysis to operate in indoor, cluttered and rough terrain environments and facilities. A set of simulation and experimental studies demonstrate the performance of the proposed solution in terms of accuracy and performance. The capacity of the method to propagate the estimated field enables accurate and reliable results even subject to short deployments which is typically the case in rapid reconnaissance and emergency response applications.

REFERENCES

[1] World Nuclear Association, "Nuclear Power in the World Today." [Online]. Available: http://www.world-nuclear.org

[2] G. Christie, A. Shoemaker, K. Kochersberger, P. Tokekar, L. McLean, and A. Leonessa, "Radiation search operations using scene understanding with autonomous uav and ugv," *Journal of Field Robotics*, 2016.

[3] M. Maimone, L. Matthies, J. Osborn, E. Rollins, J. Teza, and S. Thayer, "A photo-realistic 3-d mapping system for extreme nuclear environments: Chernobyl," in *Intelligent Robots and Systems, 1998. Proceedings., 1998 IEEE/RSJ International Conference on*, vol. 3. IEEE, 1998, pp. 1521–1527.

[4] R. Guzman, R. Navarro, J. Ferre, and M. Moreno, "Rescuer: Development of a modular chemical, biological, radiological, and nuclear robot for intervention, sampling, and situation awareness," *Journal of Field Robotics*, vol. 33, no. 7, pp. 931–945, 2016.

[5] J. Towler, B. Krawiec, and K. Kochersberger, "Radiation mapping in post-disaster environments using an autonomous helicopter," *Remote Sensing*, vol. 4, no. 7, pp. 1995–2015, 2012.
[6] K. D. Jarman, E. A. Miller, R. S. Wittman, and C. J. Gesh, "Bayesian radiation source localization," *Nuclear technology*, vol. 175, no. 1, pp. 326–334, 2011.
[7] H. Wan, T. Zhang, and Y. Zhu, "Detection and localization of hidden radioactive sources with spatial statistical method," *Annals of Operations Research*, vol. 192, no. 1, pp. 87–104, 2012.
[8] H. E. Baidoo-Williams, "Maximum likelihood localization of radiation sources with unknown source intensity," *arXiv preprint arXiv:1608.00427*, 2016.
[9] H. E. Baidoo-Williams, R. Mudumbai, E. Bai, and S. Dasgupta, "Some theoretical limits on nuclear source localization and tracking," in *Information Theory and Applications Workshop (ITA), 2015*. IEEE, 2015, pp. 270–274.
[10] G. Cordone, R. R. Brooks, S. Sen, N. S. Rao, C. Q. Wu, M. L. Berry, and K. M. Grieme, "Improved multi-resolution method for mle-based localization of radiation sources," in *Information Fusion (Fusion), 2017 20th International Conference on*. IEEE, 2017, pp. 1–8.
[11] S. Martínez, "Distributed interpolation schemes for field estimation by mobile sensor networks," *IEEE Transactions on Control Systems Technology*, vol. 18, no. 2, pp. 491–500, 2010.
[12] Y. Wang and P. Ishwar, "Distributed field estimation with randomly deployed, noisy, binary sensors," *IEEE Transactions on Signal Processing*, vol. 57, no. 3, pp. 1177–1189, 2009.
[13] H. M. La and W. Sheng, "Distributed sensor fusion for scalar field mapping using mobile sensor networks," *IEEE Transactions on cybernetics*, vol. 43, no. 2, pp. 766–778, 2013.
[14] C. Zhang, D. Arnold, N. Ghods, A. Siranosian, and M. Krstic, "Source seeking with non-holonomic unicycle without position measurement and with tuning of forward velocity," *Systems & control letters*, vol. 56, no. 3, pp. 245–252, 2007.
[15] S. Pang and J. A. Farrell, "Chemical plume source localization," *IEEE Transactions on Systems, Man, and Cybernetics, Part B (Cybernetics)*, vol. 36, no. 5, pp. 1068–1080, 2006.
[16] C. G. Mayhew, R. G. Sanfelice, and A. R. Teel, "Robust source-seeking hybrid controllers for autonomous vehicles," in *American Control Conference, 2007. ACC'07*. IEEE, 2007, pp. 1185–1190.
[17] R. A. Cortez, H. G. Tanner, and R. Lumia, "Distributed robotic radiation mapping," in *Experimental Robotics*. Springer, 2009, pp. 147–156.
[18] A. A. R. Newaz, S. Jeong, H. Lee, H. Ryu, N. Y. Chong, and M. T. Mason, "Fast radiation mapping and multiple source localization using topographic contour map and incremental density estimation," in *Robotics and Automation (ICRA), 2016 IEEE International Conference on*. IEEE, 2016, pp. 1515–1521.
[19] K. Vetter, D. Chivers, and B. Quiter, "Advanced concepts in multi-dimensional radiation detection and imaging," in *Nuclear Threats and Security Challenges*. Springer, 2015, pp. 179–192.
[20] A. A. R. Newaz, S. Jeong, H. Lee, H. Ryu, and N. Y. Chong, "Uav-based multiple source localization and contour mapping of radiation fields," *Robotics and Autonomous Systems*, vol. 85, pp. 12–25, 2016.
[21] F. Mascarich, T. Wilson, C. Papachristos, and K. Alexis, "Radiation source localization in gps-denied environments using aerial robots," in *IEEE International Conference on Robotics and Automation (ICRA)*, May 2018.
[22] J. Zhang and S. Singh, "Loam: Lidar odometry and mapping in real-time." in *Robotics: Science and Systems*, vol. 2, 2014, p. 9.
[23] P. Fankhauser and M. Hutter, "A Universal Grid Map Library: Implementation and Use Case for Rough Terrain Navigation," in *Robot Operating System (ROS) The Complete Reference (Volume 1)*, A. Koubaa, Ed. Springer, 2016, ch. 5.
[24] P. Fankhauser, M. Bloesch, and M. Hutter, "Probabilistic terrain mapping for mobile robots with uncertain localization," *IEEE Robotics and Automation Letters (RA-L)*, vol. 3, no. 4, pp. 3019–3026, 2018.
[25] P. Fankhauser, M. Bloesch, C. Gehring, M. Hutter, and R. Siegwart, "Robot-centric elevation mapping with uncertainty estimates," in *International Conference on Climbing and Walking Robots (CLAWAR)*, 2014.
[26] F. Mascarich, C. Papachristos, T. Wilson, and K. Alexis, "Distributed Radiation Field Estimation Dataset." [Online]. Available: https://github.com/unr-arl/drm_dataset